Clinical and Translational Radiation Oncology 39 (2023) 100563

Contents lists available at ScienceDirect

Clinical and Translational Radiation Oncology

journal homepage: www.sciencedirect.com/journal/clinical-and-translational-radiation-oncology

Oxygen-enhanced MRI and radiotherapy in patients with oropharyngeal squamous cell carcinoma

Emma Bluemke [a,*], Ambre Bertrand [a], Kwun-Ye Chu [b,c], Nigar Syed [b], Andrew G. Murchison [e], Rosie Cooke [b,c], Tessa Greenhalgh [b,d], Brian Burns [f], Martin Craig [g], Nia Taylor [e], Ketan Shah [b,c], Fergus Gleeson [e], Daniel Bulte [a]

[a] Institute of Biomedical Engineering, Department of Engineering Science, University of Oxford, UK
[b] MRC Oxford Institute for Radiation Oncology, Department of Oncology, University of Oxford, UK
[c] Radiotherapy Department, Oxford University Hospitals NHS Foundation Trust, UK
[d] University Hospital Southampton NHS Foundation Trust, UK
[e] Department of Radiology, Oxford University Hospitals NHS Foundation Trust, UK
[f] GE Healthcare CA, USA
[g] University of Nottingham, UK

ARTICLE INFO

Keywords:
Oxygen-enhanced MRI
Oropharyngeal squamous cell carcinoma
MRI
Oxygen
Hypoxia

ABSTRACT

Background and purpose: This study aimed to assess the role of T1 mapping and oxygen-enhanced MRI in patients undergoing radical dose radiotherapy for HPV positive oropharyngeal cancer, which has not yet been examined in an OE-MRI study.
Materials and methods: Variable Flip Angle T1 maps were acquired on a 3T MRI scanner while patients (n = 12) breathed air and/or 100 % oxygen, before and after fraction 10 of the planned 30 fractions of chemoradiotherapy ('visit 1' and 'visit 2', respectively). The analysis aimed to assess to what extent (1) native R1 relates to patient outcome; (2) OE-MRI response relates to patient outcome; (3) changes in mean R1 before and after radiotherapy related to clinical outcome in patients with oropharyngeal squamous cell carcinoma.
Results: Due to the radiotherapy being largely successful, the sample sizes of non-responder groups were small, and therefore it was not possible to properly assess the predictive nature of OE-MRI. The tumour R1 increased in some patients while decreasing in others, in a pattern that was overall consistent with the underlying OE-MRI theory and previously reported tumour OE-MRI responses. In addition, we discuss some practical challenges faced when integrating this technique into a clinical trial, with the aim that sharing this is helpful to researchers planning to use OE-MRI in future clinical studies.
Conclusion: Altogether, these results suggest that further clinical OE-MRI studies to assess hypoxia and radiotherapy response are worth pursuing, and that there is important work to be done to improve the robustness of the OE-MRI technique in human applications in order for it to be useful as a widespread clinical technique.

Introduction

Head & neck cancer is the seventh most common cancer type in the UK, and 90 % are squamous cell carcinomas with oropharyngeal being the most commonly affected subsite [1]. Although survival rates have been improving, 5-year relative survival rates are 52 % and patients undergoing treatment with radiotherapy and surgery may suffer significant morbidity as a result of treatment [2]. Since imaging is a vital component of the head and neck cancer management pathway – used for diagnosis, staging, treatment planning and response assessment – it would be ideal if an imaging biomarker could identify which tumours are less likely to respond to treatment. This would provide an opportunity to target these tumours or tumour regions using Intensity Modulated Radiotherapy (IMRT) or adaptive RT, or to use appropriate targeted radiosensitizers to improve treatment response.

One common feature in solid tumours linked to chemo- and radioresistance is low tissue oxygen levels, known as hypoxia, caused by a combination of immature vasculature, poor perfusion, and high

* Corresponding author at: Old Road Campus Research Building, University of Oxford, Headington, Oxford OX3 7DQ, UK.
E-mail address: emma.bluemke@new.ox.ac.uk (E. Bluemke).

https://doi.org/10.1016/j.ctro.2022.100563
Received 29 March 2022; Received in revised form 8 December 2022; Accepted 14 December 2022
Available online 17 December 2022

metabolic activity in the tumour [3–5]. In addition, hypoxia studies using positron emission tomography (PET) imaging have found that the persistence of hypoxia throughout chemoradiotherapy is predictive of patient clinical outcome [6,7]. In this study, we hypothesized that tumours with poor perfusion or hypoxia would be more likely to be at risk of relapse and examined the feasibility of a technique known as oxygen-enhanced MRI (OE-MRI) to provide indicators of tumour perfusion in this clinical setting [8–19].

Oxygen-enhanced MRI is a non-invasive imaging technique based on the knowledge that molecular oxygen is paramagnetic, and that the longitudinal relaxation rate R1 (1/T1) of a material will increase linearly with an increased concentration or partial pressure of oxygen (PO_2) [20–30]. If a patient inhales 100 % oxygen or carbogen, the R1 of tissues that increase in PO_2 will therefore increase, or show "oxygen-enhancement". By acquiring a measurement of R1 under normal conditions and then performing a second measurement (or dynamic measurements) while the patient is breathing an increased inspired fraction of oxygen via a face mask, the change – or absence of change – in R1 has been used to infer information about the delivery of oxygen in that tissue. In some OE-MRI studies, additional data such as changes in relaxation rate R2* (1/T2*) can also provide important information about the changes in oxygenation [9,14,31–34], and certain indicators of vasculature from dynamic contrast-enhanced MRI (DCE-MRI) have been used to distinguish between tumour regions that show no oxygen-enhancement but do show vasculature (called "Perfused Oxy-Refractory") [14,16,18]. After showing promising results in preclinical studies measuring hypoxia [9,10,13,14,16,19] or radiation response [12,18,35,36], the OE-MRI methodology has continued to be refined for clinical applications, with some analysis techniques being proposed to improve the signal-to-noise ratio, acquisition time, and to improve the robustness of the technique for use in human patients [11,15]. To date, 8 human studies have used variations of the OE-MRI method in tumours: 4 patients with brain metastasis and glioma [34], 5 patients with glioblastoma [13], 6 patients with renal carcinoma [14], 7 patients with intracranial tumours [37], 7–9 patients with anal squamous cell carcinoma [38], 10 patients with brain metastasis [17], 10 patients with cervical and hepatocellular carcinoma or metastases from ovarian and colorectal carcinomas [39], and 15 patients with non small cell lung cancer [18], with 3 of the 8 studies involving any radiotherapy treatment. In each case, the OE-MRI method has repeatedly been shown to be well-tolerated by patients.

The data presented in this manuscript is the tertiary outcome of a clinical study where the objective of this outcome was to assess the role of T1 mapping and OE-MRI techniques in patients undergoing radical dose radiotherapy (with or without systemic therapy) for HPV positive oropharyngeal cancer, which has not yet been examined in an OE-MRI study. The analysis aimed to assess to what extent (1) native R1 relates to patient outcome; (2) OE-MRI response relates to patient outcome; (3) changes in mean R1 before and after radiotherapy related to clinical outcome in patients with oropharyngeal squamous cell carcinoma. Due to the radiotherapy being largely successful, only 3 patients did not respond to radiotherapy, making it difficult to statistically compare the non-responder and responder groups and properly assess the predictive nature of OE-MRI or R1 changes. As a result, this study reports the changes observed, but was unable to report any correlations of these changes to the cancer outcomes. Lastly, we discuss some practical challenges faced when integrating this technique into a clinical trial, with the aim that sharing this is helpful to researchers planning to use OE-MRI in future clinical studies.

Methods

Patients and treatment

Patients included in this study were trial participants enrolled in the *Biological magnetic resonance imaging parameters in cancer* (BIOPIC) study who underwent radiotherapy for squamous cell oropharyngeal cancer in Oxford University Hospitals NHS Trust between 2017 and 2019 [40]. This study was approved by Wales Research Ethics Committee 4, Wrexham, and all patients provided written informed consent. From seeking informed consent, patients were followed until post-treatment imaging which takes place 10–12 weeks after completion of radiotherapy. The duration of patients' participation was approximately 4 months. All patients received radiotherapy prescribed at 65 Gy to primary and involved nodes and 54 Gy to elective nodal regions over 30 fractions. Eligible patients received concomitant systemic therapy with cisplatin (100 mg/m^2 3 weekly or 40 mg/m^2 weekly) or cetuximab (400 mg/m^2 loading, 250 mg/m^2 weekly). Treatment was delivered using simultaneous integrated boost volumetric modulated arc therapy (VMAT) plans with daily image guidance (Clinac iX, Varian Medical Systems, Palo Alto, USA).

MRI protocol

A group of 12 patients (age range 50–74) was scanned on a GE Discovery MR750 3T MRI scanner with HDNV coil array, in three separate sessions: before (visit 1), and after fraction 10 of the planned 30 fractions of radiotherapy (visit 2), and a followup 3 months after therapy – the study design is illustrated in Fig. 1. At each visit, the following images were acquired: T2-weighted image (SE sequence, TR = 781 ms, TE = 16.44 ms, slice thickness = 4.0 mm, slice gap = 4.5 mm, matrix 512 × 512, 19 slices); Modified Look Locker Inversion Recovery (MOLLI) [41] T1-mapping sequences (slice thickness = 10 mm, 11 inversion times, FA = 35, TR = 3.050 ms, TE = 1.332 ms, acquisition time approximately 15 s) acquired in a single transverse slice through the tumour volume (T1 was calculated using a nonlinear fit [41]); Variable Flip Angle (VFA) T1 maps via a 3D gradient echo sequence (TR = 4.000 ms, TE = 0.656 ms, matrix = 256 × 256, slice thickness = 5 mm, FA = 2, 5, 10, 15, acquisition time 3.5 min) [42] (T1 was calculated using a linear fit [42]). All T1 maps were calculated using MATLAB (MATLAB R2019, Mathworks, Natick, MA).

For OE-MRI, scans were acquired while the patient was breathing air and then again after breathing 100 % oxygen via an Intersurgical EcoLite high concentration oxygen mask. Patients were monitored until their end-tidal oxygen values reached ~70 % before the 'oxygen' images were acquired, which generally took 2–3 min. Their end-tidal oxygen levels were measured using a Respiratory Gas Analyzer ML206 and a PowerLab 4/26 (AD Instruments ltd, Dunedin, New Zealand).

Image analysis

A tumour region of interest (ROI) was delineated by an experienced oncologist for all primary tumours and any involved lymph nodes on high-resolution T2-weighted images. The ROIs were exported into the resolution and orientation of the single-slice MOLLI and of one slice in the 3D VFA T1 maps, for use in analysis using 3D Slicer [43]. In 3/12 subjects, the cancerous lymph node was used instead of the primary tumour due to the primary tumour either not existing, being obscured by an artefact, or being missed by the selected MOLLI slice. Tumour ROIs containing <50 voxels were excluded from the analysis. There was a noticeable darkening artefact across the first and last two slices on the T1 maps, and if the tumour ROI encompassed these slices, the data from those slices were excluded from the analysis. For each image, R1 was extracted (1/T1) and the descriptive statistics were calculated and the histogram distribution of R1 values within the tumour ROI was examined and reported.

The change in R1 within each ROI between (1) visit 1 and visit 2 (calculated as $\Delta R1_{v2\text{-}v1} = R1_{visit2} - R1_{visit1}$), (2) breathing air versus breathing oxygen on visit 1 (calculated as $\Delta R1_{ox\text{-}air} = R1_{ox} - 8\ R1_{air}$), and (3) breathing air versus oxygen on visit 2 ($\Delta R1_{ox\text{-}air} = R1_{ox} - R1_{air}$) was assessed in each patient individually using a two-sample Welch's unequal variance *t*-test (a = 0.05). In addition, Pearson correlation was used to estimate the correlation between native R1 correlated with

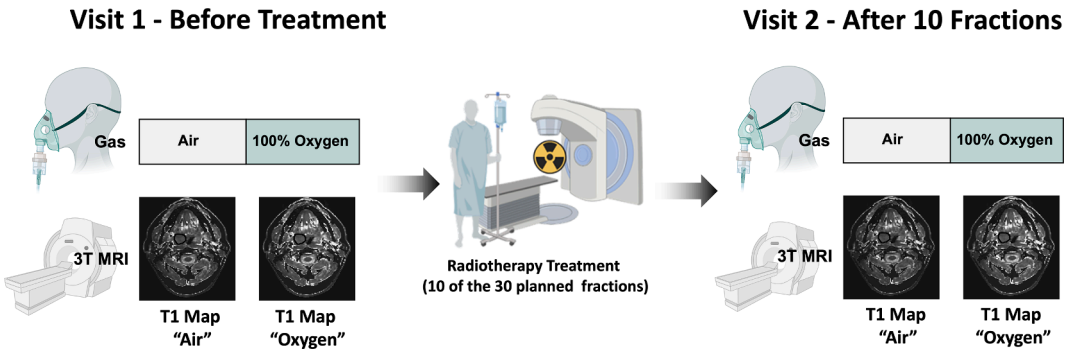

Fig. 1. The BIOPIC Trial Design. The imaging protocol was acquired while the patient was breathing air and 100% oxygen at both Visit 1 (prior to radiotherapy) and Visit 2 (after 10 of the 30 planned fractions of radiotherapy).

$\Delta R1_{ox\text{-}air}$ on either visit, or with $\Delta R1_{v2\text{-}v1}$.

At the outset of this study, the analysis of whether native T1, R1 or $\Delta R1_{ox\text{-}ai}$ related to or predicted the patient outcomes (complete response or relapse), however only 3/12 subjects did not respond to treatment, making it difficult to compare to the responder group (n = 9). The difference between the R1 of the non-responder and responder groups on each visit was assessed using a two-sample Welch's unequal variance *t*-test (a = 0.05).

Results

Resulting dataset & subject outcomes

Out of the 12 patients (age range 50–74) included in the study, Supplementary Table S1 lists the resulting dataset of acquired T1 map ROI data that passed quality control. As perhaps a cautionary tale to future researchers groups, the following obstacles were faced: (1) VFA T1 mapping was removed from protocol to cut down on scan time; (2) 4/12 MOLLI T1 maps at visit 1 were not useful due to patient motion causing the MOLLI slice to miss the tumour; (3) 8/12 MOLLI T1 maps at visit 2 were rendered unusable either from patient motion or the tumour ROI in the slice becoming very small (<50 voxels); (4) the T2* maps

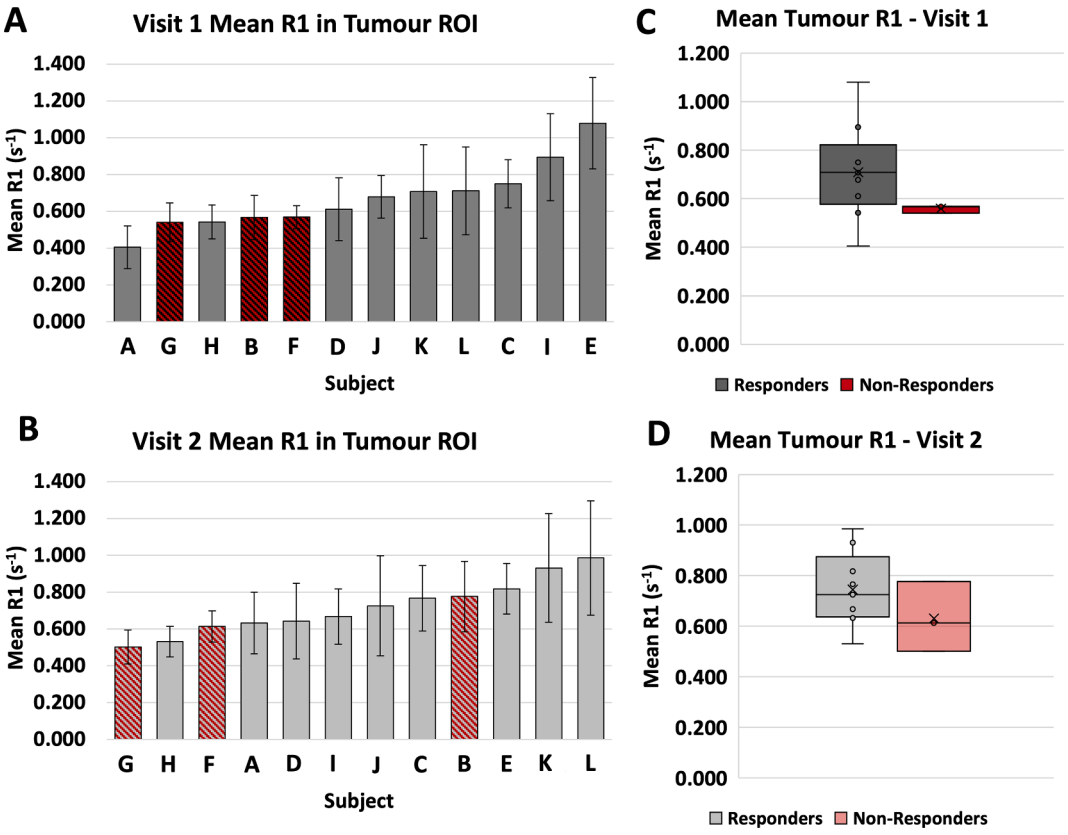

Fig. 2. *Bar graphs (A, B):* The mean R1 of the tumour ROI in all patients, visit 1 and visit 2. Patients who responded to the radiotherapy over the trial (responders) are shown in grey, patients who did not respond to treatment (non-responders) are shown in red. The error bars indicate the standard deviation of the voxel values in the ROI. *Box plots (C, D):* Box plots of the mean R1 of the tumour ROI in each group (responders n = 9, non-responders n = 3), showing a significantly higher R1 in the non-responders at visit 1 (Welch's *t*-test, two-tail $p = 0.051$) but no significant difference in R1 at visit 2. (For interpretation of the references to colour in this figure legend, the reader is referred to the web version of this article.)

acquired contained artefacts, possibly due to air in the nasal cavities, and were not able to be included in the analysis.

For the main analysis reported in this paper, the results from the analysis of the VFA T1 maps only are reported. This decision was made for two reasons: (1) the resulting dataset of VFA T1 maps was more complete for analysis, and (2) the VFA T1 maps captured the behaviour of the entire tumour, which is more indicative of the true tumour hypoxia status, while the single-slice MOLLI T1 maps captured only one slice of the tumour. A comparison of the T1 measurements provided by the MOLLI and VFA methods is beyond the scope of this manuscript and has been written up in a separate manuscript [44].

Native R1 – responders vs. non-responders

The mean tumour native R1 measurements at visit 1 and visit 2 are shown in Fig. 2, with respective histograms shown in Supplementary Fig. S1. The non-responder group (n = 3, group mean = 0.56 ± 0.02 s^{-1}) had a lower mean native R1 than the responder group (n = 9, group mean = 0.71 ± 0.19 s^{-1}) (Welch's *t*-test, two-tail $p = 0.051$). In visit 2, there was no significant difference in native R1 between groups (Welch's *t*-test, two-tail $p = 0.29$). Although it has been suggested by Akber et al. [45,46] that tissue PO_2 and longitudinal relaxation and correlates between various organs, a number of other factors can influence the R1 of a tissue, such as tissue structures, the chemical environment, pH, and the presence of blood or fat. Therefore, native R1 may not be a reliable indicator of tissue PO_2, however Cao-Pham et al. [36] have reported a general observation that a faster R1 corresponded to a more well oxygenated tumour tissue [36]. Consequently, this result could be interpreted as suggesting that the responder group contained more well-oxygenated tumour tissues (and hence faster R1) than the non-responder group at the initial visit prior to therapy.

OE-MRI response

Table 1 lists the main resulting statistics from the ROI analysis: image-derived parameters on visit 1 and visit 2 for each subject: mean R1 on air and 100 % oxygen inhalation, calculated $\Delta R1_{ox\text{-}air}$ and $\Delta R1_{v2\text{-}v1}$. For each image, the descriptive statistics are reported fully in Supplementary Table S2 and the histogram distribution of tumour R1 values within the tumour ROI are reported in Supplementary Fig. S2. For visualization, the mean R1 in the tumour ROIs while the patient was breathing air versus 100 % oxygen for visit 1 and visit 2 are plotted in Fig. 3. Across subjects, the $\Delta R1_{ox\text{-}air}$ did not correlate with native R1 on either visit (R^2 = 0.16 and 0.10 for visit 1 and visit 2, respectively, shown in Supplementary Fig. S3).

At baseline, prior to receiving radiotherapy (visit 1), there was a significant increase in R1 of the whole tumour ROIs across 3 out of 4 patients who later responded to treatment (1/4 had no significant change). There was no significant change in tumour R1 in the one patient who did not respond to treatment. After receiving 10 fractions of radiotherapy (visit 2), 3 out of 4 patients who responded to treatment showed a significant increase in tumour R1, 1/4 showed a significant decrease in tumour R1. The non-responder tumour ROI showed a significant increase in R1. These changes are shown in Fig. 3.

R1 before and after treatment

The mean R1 in the tumour ROIs on visit 1 vs. visit 2 is shown in Fig. 4 – no trend was seen between either group's changes between visits. However, the change in native R1 before and after radiotherapy ($\Delta R1_{v2\text{-}v1}$) across all patients showed a weak linear correlation with baseline native R1 (Pearson correlation, n = 12, $R^2 = 0.42$, Significance F = 0.02), in roughly 3 clusters: lower native R1 with an increase in R1 at visit 2, a medium native R1 with little to no change in R1 at visit 2, and a faster native R1 with a decrease in R1 at visit 2. Notably, these clusters did not correlate with response groupings (non-responding vs responding).

Discussion

The objective of this study was to assess to what extent (1) native R1 relates to patient outcome; (2) OE-MRI response relates to patient outcome; (3) changes in mean R1 before and after radiotherapy related to clinical outcome in patients with oropharyngeal squamous cell carcinoma. Due to the radiotherapy being largely successful, only 3 patients did not respond to radiotherapy, making it difficult to statistically compare the non-responder and responder groups and properly assess the predictive nature of OE-MRI or R1 changes. As a result, this study reports the changes observed, but was unable to report any correlations of these changes to the cancer outcomes. Nevertheless, we have reported our observations, which are useful to contribute to the current 8 OE-MRI studies in human patients, only 3 of which examined concurrent radiotherapy response thus far.

First, while the native R1 was not *predictive* of patient outcome, the responder group contained a faster R1 than the non-responder group at the initial visit prior to therapy, which is consistent with observations by Cao-Pham et al. [36] that a faster R1 corresponded to a more well oxygenated tumour tissue [36] and hence less likely to relapse. Second, it was not possible to assess the predictive nature of the OE-MRI response due to the small remaining sample size, however the majority (3 of 4) responders showed a positive $\Delta R1_{ox\text{-}air}$ while the non-responder showed no significant change in $\Delta R1_{ox\text{-}air}$. This lack of oxygen-enhancement has been suggested to be indicative of a higher percentage of hypoxic region in the tumour: Salem et al. [18] recently

Table 1
Image-derived parameters from the VFA T1 maps on visit 1 and visit 2 for each subject: mean R1 (s^{-1}) on air and 100% oxygen inhalation, calculated ΔR1 (s^{-1}), and DCE-MRI parameters.

		Visit 1				Visit 2					
		Oxygen-Enhanced MRI				Oxygen-Enhanced MRI				R1 change over Visit 1 – Visit 2	
Sub	Resp	R1 (s^{-1}) air	R1 (s^{-1}) ox	ΔR1 (s^{-1}) (ox-air)	*p*-Value	R1 (s^{-1}) air	R1 (s^{-1}) ox	ΔR1 (s^{-1}) (ox-air)	*p*-Value	ΔR1 (s^{-1}) (v2-v1)	*p*-Value
A	1	0.405	0.446	0.041	<0.0001	0.633	0.620	−0.013	<0.0001	0.228	<0.0001
B	0	0.566	0.566	0.000	0.94	0.776	0.813	0.037	<0.0001	0.210	<0.0001
C	1	0.750	0.758	0.008	<0.001	0.766	0.749	−0.017	<0.0001	0.017	<0.0001
D	1	0.611	0.719	0.108	<0.0001	0.642	0.658	0.016	<0.0001	0.031	<0.0001
E	1	1.079	1.078	−0.001	0.91	0.818	0.833	0.015	<0.0001	−0.261	<0.0001
F	0	0.568	\	\	\	0.613	\	\	\	0.045	<0.001
G	0	0.540	\	\	\	0.502	\	\	\	−0.039	<0.0001
H	1	0.542	\	\	\	0.530	\	\	\	−0.012	<0.0001
I	1	0.894	\	\	\	0.668	\	\	\	−0.227	<0.0001
J	1	0.678	\	\	\	0.725	\	\	\	0.047	<0.0001
K	1	0.707	\	\	\	0.931	\	\	\	0.224	<0.0001
L	1	0.711	\	\	\	0.986	\	\	\	0.274	<0.0001

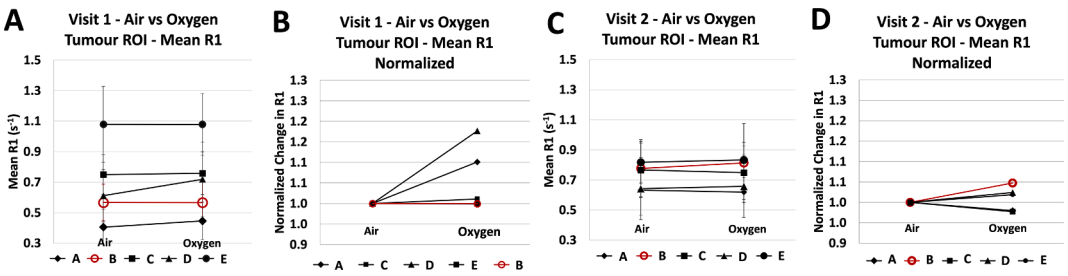

Fig. 3. The mean R1 in the tumour ROIs while the patient was breathing air versus 100% oxygen for visit 1 (A, B) and visit 2 (C, D). Graphs (B) and (D) show the corresponding % change treating native R1 as baseline. The non-responder is marked in red. (For interpretation of the references to colour in this figure legend, the reader is referred to the web version of this article.)

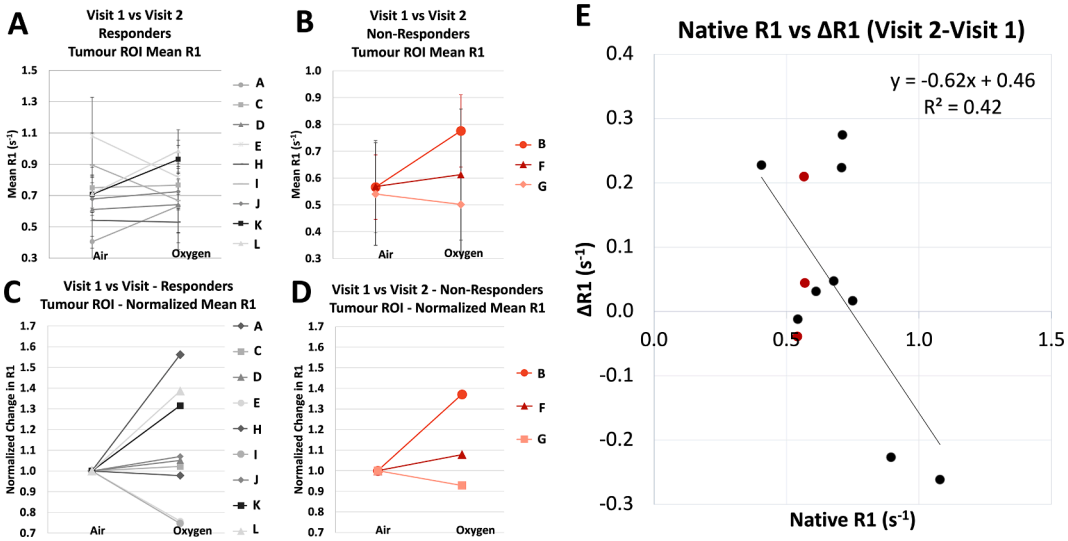

Fig. 4. The mean R1 in the tumour ROIs on visit 1 vs visit 2, (A) for the responder group and (B) non-responder group (in red). The error bars indicate the standard deviation of the voxel values in the ROI. Graphs (C) and (D) show the corresponding % change treating native R1 as baseline. (E) The change in native R1 before and after radiotherapy across all patients showed a weak linear correlation with baseline native R1 (Pearson correlation, n = 12, $R^2 = 0.42$, Significance F = 0.02). (For interpretation of the references to colour in this figure legend, the reader is referred to the web version of this article.)

reported 3 patterns of tumour response in their patients with non-small cell lung cancer: (1) a positive $\Delta R1_{ox\text{-}air}$ with a similar magnitude as seen in the aorta $\Delta R1_{ox\text{-}air}$, which corresponded to containing no "Perfused Oxy-R" regions, (2) an overall $\Delta R1_{ox\text{-}air}$ that is partially attenuated compared with the aorta $\Delta R1_{ox\text{-}air}$, which corresponded to spatially coherent regions of "Perfused Oxy-R", and (3) a non-significant $\Delta R1_{ox\text{-}air}$ response, which corresponded to a proportion of "Perfused Oxy-R", which was found to correlate with hypoxia [18]. In visit 2, one of the tumours in the "responders" group showed a net negative $\Delta R1_{ox\text{-}air}$, which has been observed previously in tumours following a gas challenge [9,11,13,17,32,34]. The source of the *negative* change in R1 is hypothesized to be due to paramagnetic deoxyhemoglobin [47]: prior to full oxygen saturation in the blood, the main source of R1 change is caused by changing levels of deoxyhemoglobin, since there is a linear relationship between the R1 of the blood and deoxyhemoglobin concentration (hence inversely linear with SO_2) [47,48]. Following full oxygen saturation, however – once deoxyhemoglobin levels no longer change – the paramagnetism of the dissolved oxygen is the dominant remaining effect on R1 change, and the R1 of blood increases linearly with increasing plasma PO_2 [26,47,49], thus showing the expected positive oxygen-enhancement. Therefore, a negative ΔR1 has been interpreted as a sign of hypoxic tissue, since hypoxic tissue will have a high concentration of deoxyhemoglobin at baseline, and will then have a large increase in SO_2 without a large change in dissolved oxygen levels [13,32].

In visit 2, the non-responder did show a positive $\Delta R1_{ox\text{-}air}$, unlike in visit 1. This positive $\Delta R1_{ox\text{-}air}$ could be interpreted as a decrease in hypoxia in comparison to the visit 1, which is not consistent with previous hypoxia studies using PET imaging that indicate that the *persistence* of hypoxia throughout chemoradiotherapy was more predictive of patient clinical outcome than the initial hypoxia levels [6,7]. However, well-perfused regions are not the only situation where a positive $\Delta R1_{ox\text{-}air}$ has been observed – when paired with an positive ΔR2*, a positive ΔR1 has been found in tissues with high fluid content such as edema, necrotic areas and CSF [34,50]. Remmele et al. [34] hypothesized that this is due to perfusion with a greatly reduced number of erythrocytes (hence no decrease in R2* as expected from decrease in deoxyhemoglobin), therefore resulting in dissolved oxygen being the dominant effect. Unfortunately, the T2* maps in this study were excluded due to artefacts, so it was not possible to discern the underlying source of this positive $\Delta R1_{ox\text{-}air}$ observed in the non-responder, however this demonstrates the importance of the inclusion of other measurements in the MRI protocol such as R2*. Therefore, although this study contained a small sample size (n = 5, other published OE-MRI clinical data has contained 4 [34], 5 [13], 6 [14], 7 [37], 7–9 [38], 10 [17], and 15 [18] subjects), the OE-MRI responses observed were consistent with the underlying OE-MRI theory and previously reported tumour OE-MRI responses.

Over the years, OE-MRI studies have used a variety of methods to detect the change in R1 – some have used semi-quantitative signal intensity changes in T1-weighted imaging [12,19,35,51,52], and some have used quantitative T1 mapping methods such as inversion recovery [13,22,25,53–55], saturation recovery [56], VFA [11,17–19,39,50,57],

or Look-Locker variants such as MOLLI [28,34,38,58,59]. There are tradeoffs between T1 estimation accuracy and acquisition time between each of these methods, and some are known to overestimate (VFA) or underestimate (Look-Locker variants) the true T1 of the material [60], with inversion recovery being the 'gold-standard' technique. Applying OE-MRI into a clinical trial workflow heightens the importance of two relevant factors: acquisition time and patient motion. Patient motion is especially detrimental if the original region of interest moves out of the imaging field-of-view, which has also occurred in previous OE-MRI studies using 2D rather than 3D imaging techniques [38,61]. In this current study, patient motion was a nontrivial concern: patient motion in the z-plane occurred in 7/12 patients, resulting in the MOLLI T1 map capturing a different section of the tumour, rendering it unusable for OE-MRI analysis. Therefore, although MOLLI provides a rapid, accurate method for T1 mapping that is appropriate for applications such as cardiac imaging, 3D T1 mapping techniques are more appropriate for capturing OE-MRI response in tumours. Acquisition time was also a relevant issue for this cohort of patients, and as the study progressed, some patients needed shorter scan time and therefore some sequences (such as those necessary for VFA post-oxygen) were removed from the protocol in order to satisfy this, reducing our OE-MRI sample size. Overall, this study intended to test the feasibility of using OE-MRI in clinical head and neck cancers, and our experience suggests that there are several challenges to successfully obtaining OE-MRI measurements in this particular application.

Most OE-MRI studies in tumours have traditionally reported changes in R1 across a whole tumour ROI, however some recent research has suggested that categorizing the *fraction* of voxels that *do* or *do not* show oxygen-enhancement may better capture the tissue heterogeneity in tumours – since some tumour regions show a positive $\Delta R1_{ox\text{-}air}$ and some show a negative $\Delta R1_{ox\text{-}air}$ [13,33], the net R1 response can cancel-out at the level of a tumour-wise measurement. Across different studies and research groups, a range of *fractional* measurements have been used: Linnik et al. [13] assessed the proportion of the tumour exhibiting a *negative area-under-the-curve* response in T1-weighted images; O'Connor et al [16] categorized voxels as oxygen-enhancing ("Oxy-E") if the voxel delta R1 was positive and significant, and all other voxels as oxygen-refractory ("Oxy-R"), and used indicators of perfusion from DCE-MRI to distinguish between "perfused Oxy-R", "non-perfused Oxy-R", and "perfused Oxy-E" regions; and Fan et al [10] derived the percent signal intensity change ("PSIC") from the T1-weighted OE-MRI response and calculated the percentage of tumour area with "high PSIC" (PSIC $>$ 10 %) and "low PSIC" (PSIC $<$ 10 %). However, successfully obtaining a voxel-wise or fractionated measurement from OE-MRI requires highly reliable alignment of voxels between the air and oxygen images, which can be difficult to achieve: patients must breathe during the gas challenge, images are acquired minutes apart, and therefore the patient may voluntarily or involuntarily move throughout the session. Aside from bulk patient motion, internal organs can move during the session as well, due to involuntary motion in the bowels or even swallowing and tongue position (relevant for oropharyngeal cancers, such as in this study), causing relative motion within the body frame which can be more difficult to correct reliably with registration than bulk motion. Therefore, future work may show that a more sophisticated analysis technique is able to extract voxel-wise or fractional measurements from this data, however this was beyond the scope of this proposed clinical trial analysis.

Limitations

In addition to the small resulting OE-MRI sample size, there are several limitations to this study. First, it would have been helpful to collect aortic PO_2 measurements to confirm the expected increase in oxygen from the gas challenge. The information of blood oxygen levels after oxygen breathing is important for experiment reproducibility in further studies. In addition, in some visits, the acquisition of a B1 map was removed from the protocol due to the patient requesting less time in the scanner. The B1 maps are useful in VFA T1 mapping to correct for errors between the intended versus actual flip angle applied [62], and the removal of them in some visit protocol made it not impossible to use B1 correction in any T1 maps, likely resulting in less accurate T1 measurements.

Conclusion

In conclusion, this study examined the feasibility of OE-MRI to provide indicators of tumour perfusion in patients with head and neck tumours. Due to the radiotherapy being largely successful, the sample sizes of non-responder groups were small, and therefore it was not possible to properly assess the predictive nature of OE-MRI. Nevertheless, the results observed were consistent with the underlying OE-MRI theory and previously reported tumour OE-MRI responses. Altogether, these results suggest that further clinical OE-MRI studies to assess hypoxia and radiotherapy response are worth pursuing, and that there is important work to be done to improve the robustness of the OE-MRI technique in human applications in order for it to be useful as a widespread clinical technique.

Declaration of Competing Interest

The authors declare that they have no known competing financial interests or personal relationships that could have appeared to influence the work reported in this paper.

Acknowledgments

This study is part of the translational cancer research programme of the University of Oxford and the Oxford University Hospitals NHS Trust. It is undertaken via the core clinical and research infrastructure underpinned by strategic research programme grant funds. The research imaging is enabled by funding provided by the Oxford Cancer Imaging Centre (OCIC). OCIC is funded by a strategic initiative from Cancer Research UK jointly with the Engineering & Physical Sciences Research Council, the Medical Research Council and the Department of Health. Funding has also been provided by the Oxfordshire Health Services Research Committee (OHSRC), a subcommittee of the Oxford Radcliffe Charitable Funds Charity. We acknowledge support provided by The CRUK Oxford Cancer Research Centre and The Oxford National Institute for Health Research Biomedical Research Centre. This work was supported by funding from the Engineering and Physical Sciences Research Council (EPSRC) and Medical Research Council (MRC) [Grant No. EP/L016052/1], the Clarendon Scholarship fund and the Joe Todd Engineering Award from St. Edmund Hall.

Appendix A. Supplementary data

Supplementary data to this article can be found online at https://doi.org/10.1016/j.ctro.2022.100563.

References

[1] Macmillan Cancer Support. The rich picture: people with head and neck cancer. 2017.
[2] Oxford Cancer Intelligence Unit. Profile of head and neck cancers in England: incidence, mortality and survival. NHS; 2010.
[3] Bader SB, Dewhirst MW, Hammond EM. Cyclic hypoxia: an update on its characteristics, methods to measure it and biological implications in cancer. Cancers 2020;13(1):23. https://doi.org/10.3390/cancers13010023.
[4] Bayer C, Shi K, Astner ST, Maftei C-A, Vaupel P. Acute versus chronic hypoxia: why a simplified classification is simply not enough. Int J Radiat Oncol Biol Phys 2011; 80(4):965–8. https://doi.org/10.1016/j.ijrobp.2011.02.049.
[5] Horsman M, Mortensen L, reviews Clinical P-J. In: Imaging hypoxia to improve radiotherapy outcome; 2012. https://doi.org/10.1038/nrclinonc.2012.171.
[6] Zips D, et al. Exploratory prospective trial of hypoxia-specific PET imaging during radiochemotherapy in patients with locally advanced head-and-neck cancer.

Radiother Oncol 2012;105(1):21–8. https://doi.org/10.1016/j.radonc.2012.08.019.
[7] Löck S, et al. Residual tumour hypoxia in head-and-neck cancer patients undergoing primary radiochemotherapy, final results of a prospective trial on repeat FMISO-PET imaging. Radiother Oncol 2017;124(3):533–40. https://doi.org/10.1016/j.radonc.2017.08.010.
[8] Cao-Pham T-T, et al. Combined endogenous MR biomarkers to assess changes in tumor oxygenation induced by an allosteric effector of hemoglobin. NMR Biomed 2019;33(2):e4181.
[9] Cao-Pham T, et al. Combined endogenous MR biomarkers to predict basal tumor oxygenation and response to hyperoxic challenge. NMR Biomed 2017;30(12):e3836.
[10] Fan Q, et al. Investigation of hypoxia conditions using oxygen-enhanced magnetic resonance imaging measurements in glioma models. Oncotarget 2017;5:31864–75. https://doi.org/10.18632/oncotarget.16256.
[11] Featherstone AK, et al. Data-driven mapping of hypoxia-related tumor heterogeneity using DCE-MRI and OE-MRI. Magn Reson Med 2017;79(4):2236–45. https://doi.org/10.1002/mrm.26860.
[12] Hallac RR, et al. Correlations of noninvasive BOLD and TOLD MRI with pO2 and relevance to tumor radiation response. Magn Reson Med 2014;71(5):1863–73. https://doi.org/10.1002/mrm.24846.
[13] Linnik IV, et al. Noninvasive tumor hypoxia measurement using magnetic resonance imaging in murine U87 glioma xenografts and in patients with glioblastoma. Magn Reson Med 2014;71(5):1854–62. https://doi.org/10.1002/mrm.24826.
[14] Little RA, et al. Mapping hypoxia in renal carcinoma with oxygen-enhanced MRI: comparison with intrinsic susceptibility MRI and pathology. Radiology 2018;288(3):739–47. https://doi.org/10.1148/radiol.2018171531.
[15] Moosvi F, Baker JHE, Yung A, Kozlowski P, Minchinton AI, Reinsberg SA. Fast and sensitive dynamic oxygen-enhanced MRI with a cycling gas challenge and independent component analysis. Magn Reson Med 2018;81(4):2514–25. https://doi.org/10.1002/mrm.27584.
[16] O'Connor J, et al. Oxygen-enhanced MRI accurately identifies, quantifies, and maps tumor hypoxia in preclinical cancer models. Cancer Res 2016;76(4):787–95. https://doi.org/10.1158/0008-5472.can-15-2062.
[17] Qian J, et al. In vivo monitoring of oxygen levels in human brain tumor between fractionated radiotherapy using oxygen-enhanced MR imaging. Curr Med Imaging Former Curr Med Imaging Rev 2020;16(4):427–32. https://doi.org/10.2174/1573405614666180925144814.
[18] Salem A, et al. Oxygen-enhanced MRI is feasible, repeatable, and detects radiotherapy-induced change in hypoxia in xenograft models and in patients with non-small cell lung cancer. Clin Cancer Res 2019;25(13):3818–29. https://doi.org/10.1158/1078-0432.ccr-18-3932.
[19] Zhou H, et al. Examining correlations of oxygen sensitive MRI (BOLD/TOLD) with [18F]FMISO PET in rat prostate tumors. Am J Nucl Med Mol Imaging 2019;9(2):156–67.
[20] Vatnehol SAS, Hol PK, Bjørnerud A, Amiry-Moghaddam M, Haglerød C, Storås TH. Determination of oxygen r1 at 3 Tesla using samples with a concentration range of dissolved oxygen. Magn Reson Mater Phys Biol Med 2020;33(3):447–53. https://doi.org/10.1007/s10334-019-00783-x.
[21] Nestle N, Baumann T, Niessner R. Oxygen determination in oxygen-supersaturated drinking waters by NMR relaxometry. Water Res 2003;37(14):3361–6. https://doi.org/10.1016/S0043-1354(03)00211-2.
[22] Zaharchuk G, Martin AJ, Rosenthal G, Manley GT, Dillon WP. Measurement of cerebrospinal fluid oxygen partial pressure in humans using MRI. Magn Reson Med 2005;54(1):113–21. https://doi.org/10.1002/mrm.20546.
[23] Zaharchuk G, Busse RF, Rosenthal G, Manley GT, Glenn OA, Dillon WP. Noninvasive oxygen partial pressure measurement of human body fluids in vivo using magnetic resonance imaging. Acad Radiol 2006;13(8):1016–24. https://doi.org/10.1016/j.acra.2006.04.016.
[24] Hausser R, Noack F. Kernmagnetische Relaxation und Korrelation im System Wasser – Sauerstoff. Z Für Naturforschung A 1965;20(12):1668–75. https://doi.org/10.1515/zna-1965-1220.
[25] Simpson ARH, Dowell NG, Jackson TL, Tofts PS, Hughes EH. Measuring the effect of Pars Plana vitrectomy on vitreous oxygenation using magnetic resonance imaging effects of PPV on pO2 using MRI. Invest Ophthalmol Vis Sci 2013;54(3):2028–34. https://doi.org/10.1167/iovs.12-11258.
[26] d'Othée BJ, Rachmuth G, Munasinghe J, Lang EV. The effect of hyperoxygenation on T1 relaxation time in vitro1. Acad Radiol 2003;10(8):854–60. https://doi.org/10.1016/s1076-6332(03)00004-7.
[27] Matsumoto K, et al. MR assessment of changes of tumor in response to hyperbaric oxygen treatment. Magn Reson Med 2006;56(2):240–6. https://doi.org/10.1002/mrm.20961.
[28] Muir ER, Zhang Y, Nateras OSE, Peng Q, Duong TQ. Human vitreous: MR imaging of oxygen partial pressure. Radiology 2013;266(3):905–11. https://doi.org/10.1148/radiol.12120777.
[29] Hueckel P, Schreiber W, Markstaller K, Bellemann M, Kauczor H-U, Thelen M. Effect of partial oxygen pressure and hematocrit on T1 relaxation in human blood. Proc Int Soc Magn Reson Med 2000:1586.
[30] Chiarotti G, Cristiani G, Giulotto L. Proton relaxation in pure liquids and in liquids containing paramagnetic gases in solution. Il Nuovo Cimento 1955-1965 1955;1(5):863–73. https://doi.org/10.1007/bf02731333.
[31] Zhao D, et al. Dynamic oxygen challenge evaluated by NMR T1 and T2*–insights into tumor oxygenation. NMR Biomed 2015;28(8):937–47. https://doi.org/10.1002/nbm.3325.
[32] Burrell JS, et al. Exploring ΔR(2)* and ΔR(1) as imaging biomarkers of tumor oxygenation. J Magn Reson Imaging JMRI 2013;38(2):429–34. https://doi.org/10.1002/jmri.23987.
[33] Yang DM, Arai TJ, Campbell JW, Gerberich JL, Zhou H, Mason RP. Oxygen-sensitive MRI assessment of tumor response to hypoxic gas breathing challenge. NMR Biomed 2019;32(7):e4101.
[34] Remmele S, et al. Dynamic and simultaneous MR measurement of R1 and R2* changes during respiratory challenges for the assessment of blood and tissue oxygenation. Magn Reson Med 2013;70(1):136–46. https://doi.org/10.1002/mrm.24458.
[35] White DA, et al. Developing oxygen-enhanced magnetic resonance imaging as a prognostic biomarker of radiation response. Cancer Lett 2016;380(1):69–77. https://doi.org/10.1016/j.canlet.2016.06.003.
[36] Cao-Pham T-T, et al. Monitoring tumor response to carbogen breathing by oxygen-sensitive magnetic resonance parameters to predict the outcome of radiation therapy: a preclinical study. Int J Radiat Oncol 2016;96(1):149–60. https://doi.org/10.1016/j.ijrobp.2016.04.029.
[37] Müller A, et al. Intracranial tumor response to respiratory challenges at 3.0 T: impact of different methods to quantify changes in the MR relaxation rate R2*. J Magn Reson Imaging 2010;32(1):17–23. https://doi.org/10.1002/jmri.22205.
[38] Bluemke E, et al. Oxygen-enhanced MRI MOLLI T1 mapping during chemoradiotherapy in anal squamous cell carcinoma. Clin Transl Radiat Oncol 2020;22:44–9. https://doi.org/10.1016/j.ctro.2020.03.001.
[39] O'Connor JP, et al. Preliminary study of oxygen-enhanced longitudinal relaxation in MRI: a potential novel biomarker of oxygenation changes in solid tumors. Int J Radiat Oncol Biol Phys 2009;75(4):1209–15. https://doi.org/10.1016/j.ijrobp.2008.12.040.
[40] 'ISRCTN – ISRCTN12676704: biological magnetic resonance imaging parameters in cancer'. https://www.isrctn.com/ISRCTN12676704 [accessed Aug. 24, 2021].
[41] Messroghli DR, Radjenovic A, Kozerke S, Higgins DM, Sivananthan MU, Ridgway JP. Modified look-locker inversion recovery (MOLLI) for high-resolution T1 mapping of the heart. Magn Reson Med 2004;52(1):141–6. https://doi.org/10.1002/mrm.20110.
[42] Cheng H, in An W-G. In: Rapid high-resolution T1 mapping by variable flip angles: accurate and precise measurements in the presence of radiofrequency field inhomogeneity; 2006. https://doi.org/10.1002/mrm.20791.
[43] Fedorov A, et al. 3D Slicer as an image computing platform for the quantitative imaging network. Magn Reson Imaging 2012;30(9):1323–41. https://doi.org/10.1016/j.mri.2012.05.001.
[44] Bluemke E et al. Using variable flip angle (VFA) and modified look-locker inversion recovery (MOLLI) T1 mapping in clinical OE-MRI. *Rev*.
[45] Akber SF. Comment on "Imaging tumor hypoxia by magnetic resonance methods". J Radiother Pract 2012;11(1):66–7. https://doi.org/10.1017/S1460396911000458.
[46] Akber SF. Correlation between oxygen tension and spin-lattice relaxation rate in tumors. Eur J Radiol 1989;9(1):56–9.
[47] Silvennoinen MJ, Kettunen MI, Kauppinen RA. Effects of hematocrit and oxygen saturation level on blood spin-lattice relaxation. Magn Reson Med 2003;49(3):568–71. https://doi.org/10.1002/mrm.10370.
[48] Blockley NP, Jiang L, Gardener AG, Ludman CN, Francis ST, Gowland PA. Field strength dependence of R 1 and R2* relaxivities of human whole blood to prohance, vasovist, and deoxyhemoglobin. Magn Reson Med 2008;60(6):1313–20. https://doi.org/10.1002/mrm.21792.
[49] Pilkinton DT, Hiraki T, Detre JA, Greenberg JH, Reddy R. Absolute cerebral blood flow quantification with pulsed arterial spin labeling during hyperoxia corrected with the simultaneous measurement of the longitudinal relaxation time of arterial blood. Magn Reson Med 2012;67(6):1556–65. https://doi.org/10.1002/mrm.23137.
[50] Winter JD, Akens MK, Cheng H-L-M-L. Quantitative MRI assessment of VX2 tumour oxygenation changes in response to hyperoxia and hypercapnia. Phys Med Biol 2011;56(5):1225–42. https://doi.org/10.1088/0031-9155/56/5/001.
[51] Ohno Y, Hatabu H, Takenaka D, Adachi S, Van Cauteren M, Sugimura K. Oxygen-enhanced MR ventilation imaging of the lung: preliminary clinical experience in 25 subjects. Am J Roentgenol 2001;177(1):185–94. https://doi.org/10.2214/ajr.177.1.1770185.
[52] Ding Y, et al. Simultaneous measurement of tissue oxygen level-dependent (TOLD) and blood oxygenation level-dependent (BOLD) effects in abdominal tissue oxygenation level studies: simultaneous measurement of TOLD and BOLD. J Magn Reson Imaging 2013;38(5):1230–6. https://doi.org/10.1002/jmri.24006.
[53] Zhang W-J, Niven RM, Young SS, Liu Y-Z, Parker GJM, Naish JH. Dynamic oxygen-enhanced magnetic resonance imaging of the lung in asthma—initial experience. Eur J Radiol 2015;84(2):318–26. https://doi.org/10.1016/j.ejrad.2014.10.021.
[54] Hatabu H, et al. Pulmonary ventilation: dynamic MRI with inhalation of molecular oxygen. Eur J Radiol 2001;37(3):172–8. https://doi.org/10.1016/S0720-048X(00)00298-9.
[55] Muir ER, Cardenas DP, Duong TQ. MRI of brain tissue oxygen tension under hyperbaric conditions. Neuroimage 2016;133:498–503. https://doi.org/10.1016/j.neuroimage.2016.03.040.
[56] McGrath DM, et al. Oxygen-induced changes in longitudinal relaxation times in skeletal muscle. Magn Reson Imaging 2008;26(2):221–7. https://doi.org/10.1016/j.mri.2007.06.011.
[57] O'Connor JPB, et al. Organ-specific effects of oxygen and carbogen gas inhalation on tissue longitudinal relaxation times. Magn Reson Med 2007;58(3):490–6. https://doi.org/10.1002/mrm.21357.
[58] Kindvall SSI, Diaz S, Svensson J, Wollmer P, Olsson LE. The change of longitudinal relaxation rate in oxygen enhanced pulmonary MRI depends on age and BMI but

not diffusing capacity of carbon monoxide in healthy never-smokers. PLoS One 2017;12(5):e0177670.
[59] Vatnehol SAS, Hol PK, Bjørnerud A, Amiry-Moghaddam M, Haglerød C, Storås TH. Effect of drinking oxygenated water assessed by in vivo MRI relaxometry. J Magn Reson Imaging 2020;52(3):720–8. https://doi.org/10.1002/jmri.27104.
[60] Stikov N, Boudreau M, Levesque IR, Tardif CL, Barral JK, Pike BG. On the accuracy of T1 mapping: searching for common ground. Magn Reson Med 2015;73:514–22. https://doi.org/10.1002/mrm.25135.
[61] Morgan AR, et al. Feasibility assessment of using oxygen-enhanced magnetic resonance imaging for evaluating the effect of pharmacological treatment in COPD. Eur J Radiol 2014;83(11):2093–101. https://doi.org/10.1016/j.ejrad.2014.08.004.
[62] Boudreau M, Tardif CL, Stikov N, Sled JG, Lee W, Pike GB. B 1 mapping for bias-correction in quantitative T 1 imaging of the brain at 3T using standard pulse sequences: B 1 Maps for Quantitative T 1. J Magn Reson Imaging 2017;46(6):1673–82. https://doi.org/10.1002/jmri.25692.